Title

Evidence of an Annexin A4 mediated plasma membrane repair response to biomechanical strain associated with glaucoma pathogenesis

Journal

Journal of Cellular Physiology, 237(9)

ISSN

0021-9541

Authors

Vicic, Nevena
Guo, Xiaoxin
Chan, Darren
et al.

Publication Date

2022-09-01

DOI

10.1002/jcp.30834

Peer reviewed

Published in final edited form as:

J Cell Physiol. 2022 September ; 237(9): 3687–3702. doi:10.1002/jcp.30834.

Evidence of an Annexin A4 mediated plasma membrane repair response to biomechanical strain associated with glaucoma pathogenesis

Nevena Vicic[1,2,3], **Xiaoxin Guo**[1,2], **Darren Chan**[1,2], **John G Flanagan**[4], **Ian A. Sigal**[5], **Jeremy M. Sivak**[1,2,3]

[1]Donald K Johnson Eye Institute, Krembil Research Institute, University Health Network, Toronto, Ontario, Canada

[2]Department of Ophthalmology and Vision Science, University of Toronto School of Medicine, Toronto, Ontario, Canada

[3]Department of Laboratory Medicine and Pathobiology, University of Toronto School of Medicine, Toronto, Ontario, Canada

[4]The Herbert Wertheim School of Optometry and Vision Science, University of California Berkeley, Berkeley, California, USA

[5]Department of Ophthalmology, University of Pittsburgh, Pittsburgh, Pennsylvania, USA

Abstract

Glaucoma is a common neurodegenerative blinding disease that is closely associated with chronic biomechanical strain at the optic nerve head (ONH). Yet, the cellular injury and mechanosensing mechanisms underlying the resulting damage have remained critically unclear. We previously identified Annexin A4 (ANXA4) from a proteomic analyses of human ONH astrocytes undergoing pathological biomechanical strain that mimics glaucomatous conditions. Annexins are a family of calcium-dependent phospholipid binding proteins with key functions in plasma membrane repair (PMR); an active mechanism to limit and mend cellular injury that involves membrane and cytoskeletal reorganizations. However, a role for direct membrane damage and PMR has not been well studied in the context of biomechanical strain, such as that associated with glaucoma. Here we report that this moderate strain surprisingly damages cell membranes to increase permeability in a calcium-dependent manner, and induces rapid aggregation of ANXA4 at injury sites. ANXA4 loss-of-function increases permeability, while exogenous ANXA4 reduces it. Furthermore, ANXA4 aggregation is associated with F-actin dynamics in vitro, and remarkably this interaction and aggregation signature is also observed in the glaucomatous ONH in patient samples. Together these studies link moderate biomechanical strain with direct membrane damage and actin dynamics, and identify an active PMR role for ANXA4 in new model of cell injury associated with glaucoma pathogenesis.

Correspondence: Jeremy M. Sivak, Department of Vision Sciences, Krembil Research Institute, Krembil Discovery Tower, 60 Leonard Ave, Toronto, Ontario M5T 0S8, Canada. jsivak@uhnres.utoronto.ca.

SUPPORTING INFORMATION Additional supporting information can be found online in the Supporting Information section at the end of this article.

Keywords

Annexins; ANXA4; astrocytes; biomechanics; glaucoma; optic nerve; plasma membrane repair; stretch

1 | INTRODUCTION

Glaucoma is a progressive neurodegenerative disorder that is closely associated with elevated intraocular pressure (IOP), and a leading cause of vision loss worldwide (Weinreb et al., 2016; Zhang et al., 2021). Elevated IOP translates into increased biomechanical strain at the vulnerable optic nerve head (ONH); thought to be a principal site of early damage (Crawford Downs et al., 2011; Sigal et al., 2014; Stowell et al., 2017; Voorhees et al., 2017). This IOP-induced strain causes complex ONH tissue distortions, including compression, extension, and shear (Alqawlaq et al., 2019; Burgoyne, 2011; Sigal et al., 2007; Stowell et al., 2017). Yet, the cellular injury and mechanosensing mechanisms linking this strain to cellular damage are critically unclear, and remain a key research question. The resulting chronic strain injury induces a cascade of pathological effects that prominently include cytoskeletal remodeling and para-inflammatory activation of ONH astrocytes (Almasieh et al., 2012; Alqawlaq et al., 2019, 2020; Livne-Bar et al., 2016), which are crucial for providing structural and homeostatic support to retinal ganglion cell (RGC) axons as they exit the eye to form the optic nerve (Alqawlaq et al., 2020; Guo et al., 2018; Livne-Bar et al., 2017).

To study these glial cell responses we previously performed proteomic analyses of human ONH astrocytes undergoing pathologically relevant biomechanical strain that mimics the conditions seen in the glaucomatous environment (Exler et al., 2016; R. S. Rogers et al., 2012). A top hit in this screen was Annexin A4 (ANXA4), which was significantly increased in response to prolonged strain. This result is consistent with other work describing annexin upregulation in glaucoma, ischemic injury, Alzheimer's disease, and related neurodegenerative processes (Eberhard et al., 1994; Facio et al., 2011; Johnson et al., 2007; Kulik et al., 2009; La et al., 2001; Ries et al., 2021; Ruan et al., 2013). Similar to other Annexin family members, ANXA4 translocates to cell membranes upon elevation of intracellular calcium and forms lateral assemblies of two-dimensional (2D) trimer structures (Newman et al., 1991). This crystalline arrangement affects membrane properties such as rigidity, fluidity, and lipid domain stabilization (Piljic & Schultz, 2006; Skrahina et al., 2008), with growing evidence that ANXA4 acts as an important sensor and agent for membrane curvature during membrane repair (Boye et al., 2017; Florentsen et al., 2021; Mularski et al., 2021). Yet the impact of moderate biomechanical strain on astrocytic cell membranes is unclear, and the role of ANXA4 in any resulting injury response at the ONH has not been explored.

Plasma membrane repair (PMR) mechanisms have evolved to ensure that cell and nuclear membranes are not unduly compromised by external forces. Rapid resealing prevents unregulated calcium entry and cytoskeletal breakdown that can result in cell death (P. L. McNeil & Kirchhausen, 2005). Thus, PMR is an active process that depends on membrane

rearrangement, fusion, and extensive cytoskeletal reorganization (Horn & Jaiswal, 2018; P. L. McNeil & Steinhardt, 2003). Plasma membrane maintenance and repair has consequently been linked to a variety of physiological and pathological processes, but has proven challenging to directly link to neurodegenerative disease (Dias & Nylandsted, 2021). The Annexins form a large family of structurally related proteins that can reversibly bind to negatively charged phospholipids in a calcium-dependent manner (Gerke & Moss, 2002; Rescher & Gerke, 2004). Several Annexins play important roles in PMR processes by aggregating as 2D trimer structures at the inner membrane in a calcium-dependent manner. These assemblies prevent the damaged membrane from expanding, and direct membrane curvature and constriction to contain further damage and calcium elevation (Bouter et al., 2011; Boye et al., 2017). In addition, Annexin A2 has been shown to interact with cytoskeletal components to help reseal plasma membranes by facilitating F-actin dynamics (Jaiswal et al., 2014). Different Annexins have therefore been implicated in distinct roles in sensing and repairing membrane lesions triggered by a variety of acute cellular stresses and injuries, such as pore-forming toxins or laser irradiation (Bouter et al., 2011; Draeger et al., 2011; Jaiswal et al., 2014; A. K. McNeil et al., 2006). However, the direct involvement of PMR and Annexin 4 during strain associated with glaucomatous neurodegeneration has not been well studied.

Here we report our investigations that reveal the compromising influence of moderate pathologically relevant biomechanical strain on astrocytic cell membrane permeability and integrity, and uncover a role for ANXA4 to respond to this damage and promote repair during glaucoma pathogenesis.

2 | MATERIALS AND METHODS

2.1 | Cell culture and mechanical insults

The astroglial A7 cell line derived from neonatal rat optic nerve were maintained at 37°C with Dulbecco's H-21 media supplemented with 10% fetal bovine serum (FBS) (Multicell) and 1% penicillin/streptomycin. Human ONH astrocytes were isolated and cultured as described (R. S. Rogers et al., 2012). Previously isolated and aliquoted cells were thawed and cultured in Dulbecco's modified Eagle's medium (DMEM)/F12, supplemented with 10% FBS and 1% penicillin/streptomycin. For biomechanical stretch experiments a FlexCell® Tension Plus FX-4000T system was used to model the biomechanical environment of the ONH as reported previously (Exler et al., 2016; R. S. Rogers et al., 2012). Briefly, Bioflex plates (Flexcell) were precoated with collagen I and IV before plating cells at densities to reach 75% confluency at the time of experimental procedures. Stretch-induced insult was preceded by change to fresh media or Ca^{2+}-free DMEM/F12 media as indicated, followed by equiaxial stretch using the FlexCell system. Equiaxial stretch was applied at 12% at 1 Hz for either 1 or 5 min as indicated. Controls were plated in parallel on Bioflex plates without stretch, but otherwise treated under the identical conditions. As comparators to induce direct, focal mechanical injury two methodologies were used; (1) glass bead injury or (2) scratch assay. (1) For glass bead injury cells were plated on glass coverslips. Following a brief wash in phosphate-buffered saline (PBS), coverslips were transferred to HBSS (+10 mM HEPES, +2 mM Ca^{2+}, pH 7.4). Glass beads (425–600 μm;

Sigma) were then gently rolled onto the coverslips in all directions for 15 s. The glass beads were then washed off, followed by immediate fixation of cells in 4% paraformaldehyde (PFA). For scratch injury cells plated on coverslips were washed as described above and incubated in HBSS containing 1 mg/ml lysine fixable 10-kDa TRITC-dextran (Thermo). A 30 G needle was then carefully used to scratch the surface of the coverslip unidirectionally. Following injury cells were immediately washed in HBSS, followed by PFA fixation. Coverslips were mounted and imaged using Zeiss Confocal Microscope LSM 780 with Zen software. Additional cell treatments were applied as described in the results, consisting of ionomycin (10 μM), cytochalasin D (1.0 μM), or jasplakinolide (0.5 μM), each reconstituted in dimethyl sulfoxide (Bubb et al., 1994; Wakatsuki et al., 2001).

2.2 | Plasmid construction and small interfering RNA (siRNAs)

For overexpression studies ANXA4 coding plasmids were purchased from the SPARC BioCenter at the Hospital for Sick Children (Toronto, ON) with inserts containing a GFP tag at the C-terminal of the full human ANXA4 coding sequence. The insert was confirmed by sequencing, GFP fluorescence imaging, and western blot. Transfection with ANXA4-GFP or empty vector control was performed using Lipofectamine 3000 reagent (Thermo Fischer) following the manufacturers protocol (Supporting Information: Figure 1). For knockdown studies ON-TARGETplus SMARTpool rat ANXA4 siRNAs were obtained from Dharmacon, along with scrambled nontargeting controls (NT). Transfections of ANXA4 and NT siRNAs were performed at 20 nM into cells using DHARMAfect 1 Reagent (Dharmacon) for 48 h according to the manufacturer's directions. The magnitude of ANXA4 knockdown was assessed by quantitative real-time polymerase chain reaction (qRT-PCR) and western blot compared to NT control.

2.3 | Membrane permeability stains

Before biomechanical insult, cells were incubated with either 5 μg/ml lysine fixable FM 1–43FX (Thermo) or 3 μM cell impermeable DRAQ7™ (Cell Signaling) in Hanks Balanced Salt Solution (+10 mM HEPES, pH 7.4). Strain was applied to cells for the indicated times, washed with PBS, and then fixed with 4% PFA at 4°C. Nonstrained controls were otherwise incubated and fixed in parallel under the same conditions. Bioflex membrane bottoms were then removed and washed in PBS and mounted on slides. Cells were imaged using a Nikon Eclipse-Ti Confocal microscope with NIS Elements software.

2.4 | Western blot analysis and immunostaining

For western blot analysis, cell and tissue protein was collected in RIPA lysis buffer containing protease and phosphatase inhibitors, homogenized, and run on a 12% sodium dodecyl sulfate poly-acrylamide gel according to standard practices. The protein was then transferred onto a polyvinylidene difluoride membrane and blocked with 5% bovine serum albumin as previously described (Alqawlaq et al., 2020). Membranes were incubated with primary antibodies raised against ANXA4 (1:2000 dilution; Sigma) and glyceraldehyde 3-phosphate dehydrogenase (1:10,000 dilution; Calbiochem). This was followed by appropriate IRDye secondary antibody incubation (1:10,000; Mandel Scientific), and imaged with a LI-COR Odyssey infrared imager (BioAgilytix). Specificity of the ANXA4 antibody was confirmed by blotting with a clear knockdown of the ANXA4

band (Supporting Information: Figure 3). For immunostaining, fixed cells on coverslips were permeabilized using 0.2% triton-X in PBS. After blocking, primary antibodies to ANXA4 (1:200; Sigma), glial fibrillary acidic protein (GFAP) (1:200; Sigma), β3 tubulin (1:200; Abcam) were incubated at 4°C overnight. Samples were then incubated in Alexa-Fluor-488 or Alexa-Fluor-568 secondary antibodies (1:200; Life Technologies) for 1 h. Alexa-Fluor-647 phalloidin (1:50; Life Technologies) was incubated for 1 h, washed and coverslipped. Images were taken using a Nikon Eclips-Ti Confocal or Zeiss LSM 780 Confocal microscope. Colocalization coefficients were measured using Nikon NIS Elements Software version AR 4.51.00. Specificity of each antibody was confirmed using parallel control sections prepared with no primary antibody). In particular, the ANXA4 antibody has been previously characterized (Liu et al., 2017; Yamashita et al., 2012), and showed no background signal (Supporting Information: Figure 4).

2.5 | Recombinant ANXA4 expression and purification

The human ANXA4 gene sequence was subcloned into a pET-28a(+) bacterial expression plasmid (EMD) at Nhe1 and BamH1 sites by standard methods and transformed into competent *Escherichia coli*, cells according to the manufacturer's directions. Recombinant ANXA4 expression was induced by treatment with 1 mM IPTG. Expression of the target protein were visualized and identified by SDS-PAGE and western blot analysis. Cell pellet from large-scale culture was lysed using Bugbuster Protein Extraction Reagent (Novagen). Target protein was then purified through Ni-NTA resin column and eluted by Imidazole repetitively. Insoluble faction of the protein pellet was purified under denaturing condition. Both purification products were combined and dialysed to remove undesired reagents (Supporting Information: Figure 2). Recombinant ANXA4 was dissolved in serum-free DMEM at 5 or 50 μg/ml, along with DMEM vehicle control, and applied for 30 min to A7 cells plated on Bioflex plates for permeability experiments. Cells were then subjected to 12% cyclic mechanical stretch for 5 min, stained with FM-143FX, and imaged as described above.

2.6 | Electron microscopy

To prepare stretched monolayer cells for transmission electron microscopy (TEM) imaging: after stretch experiments, cells were fixed with 4% PFA in PBS. The silicone bottom with fixed cells was then carefully cut away from the Bioflex plate and further subdivided into squares of around 4 mm^2. Cells were washed 3× with 0.1 M cacodylate buffer and postfixed in 1% osmium tetroxide, 1.25% potassium ferrocyanide in cacodylate buffer for 1.5 h, then washed 3× with cacodylate buffer, followed by then 2× with dH_2O, and stained for 30 min with 4% aqueous uranyl acetate and washed 2× with dH_2O. Samples were then dehydrated in increasing concentrations of ethanol, followed by 2× propylene oxide for 10 min. Infiltration was performed with increasing concentrations of Spurr's resin in propylene oxide on a rotator and ending in 100% Spurr's resin overnight. The silicone membrane squares were transferred onto moulds with cells facing up and embedded in fresh Spurr's resin, placed at 65°C, and allow to polymerize for 2 days. The cured resin block was removed from the mould and the silicone membrane was gently peeled off. The silicone membrane was then checked under a phase contrast microscope to confirm that the monolayer was successfully transferred to the resin. To avoid rolling and folding of the

monolayer on the edge of ultrathin sections, the following extra steps were taken; fresh Spurr's was added to the cell interface of the resin block, allowed to polymerize, then followed by sectioning. The resin block was oriented to enable ultrathin sectioning through the monolayer. The ultrathin sections were then imaged with a T20 TEM at the Nanoscale Biomedical Imaging Facility, Sickkids Hospital. Similarly, ultrathin sections were prepared in LR White resins for immunogold labeling to detect ANXA4 using colloidal gold particles of 10 nm size conjugated secondary antibody as indicated by the manufacturer (Aurion Conventional Immunogold Reagents; Electronic Microscopy Sciences).

2.7 | ONH staining and imaging

2.7.1 | Animal studies—All animal experiments were conducted under a protocol approved by the University Health Network (UHN) animal care committee and conformed to local, provincial, and federal regulations. Wistar rats eyes were collected and sectioned as previously described (Guo et al., 2018). Briefly, p21–p30 rats were killed by CO_2 asphyxiation. Eyes were then immediately enucleated and processed for analyses. Fixed eye tissues were dehydrated using 30% sucrose overnight before OCT embedding and cryosectioning. Tissue sections were permeabilized using 0.2% triton-X in PBS. After blocking, primary antibodies to ANXA4 (1:200; Sigma), GFAP (1:200; Sigma), β3 tubulin (1:200; Abcam) were incubated overnight. Samples were then incubated in Alexa-Fluor-488 or Alexa-Fluor-568 secondary antibodies (1:200; Life Technologies) for 1 h. Rhodamine phalloidin (1:50, Life Technologies) was incubated for 1 h, washed and coverslipped. Images were taken using a Nikon Eclips-Ti Confocal Microscope.

2.7.2 | Human eye studies—Age-matched glaucomatous and control human eye sections were obtained through the Toronto Human Eye Biobank under informed consent, under a protocol approved by the UHN Research Ethics Board, and their collection and use conformed to the Declaration of Helsinki. An antigen retrieval technique was used to probe formalin-fixed paraffin-embedded human eye sections. Briefly, sections were deparaffinized by gently heating to 55°C for 10 min and washed in several xylene rinses, followed by graded washes with xylene and ethanol. Samples were then rehydrated with graded ethanol in water. Slides were then immersed in citrate buffer and placed in a Biocare Medical Decloaking Chamber set to 95°C for 10 min, followed by 90°C for 10 s. The slides were removed and cooled on the benchtop for 25 min and rinsed with PBS three times and then immunostained as above for ANXA4 and with phalloidin. As a further control, we performed a competition experiment on human sections using recombinant ANXA4 (rANXA4, Supporting Information: Figure 4). Briefly, ANXA4 antibody alone and an ANXA4ab:rANXA4 (1:3 ratio) mixture was prepared in PBS and incubated for 1 h at room temp. The mixtures were applied to prepermeabilized human eye tissue sections at 4°C overnight, followed by secondary antibody as described above. The ONH regions were imaged on a Nikon Eclips-Ti Confocal Microscope, and analyzed using Nikon NIS Elements Software version AR 4.51.00 with the counting function to measure ANXA4:actin foci per mm^2 in three LCr regions for each eye from control and glaucoma patient samples.

2.8 | Statistical analyses

Data were analyzed by Student's *t* test, or analysis of variance (ANOVA) with Tukey post hoc analyses when assessing more than two groups. Figures 1e,2e,3b,c,e, were analyzed by two-way ANOVA withTukey multiple comparisons test. Significance was determined as a $p < 0.05$, with the specific values below this threshold indicated on each chart. The number of biological replicates is reported for each experiment as "*n*."

3 | RESULTS

3.1 | ANXA4 rapidly translocates to the membrane in response mechanical injury

Experiments in acute cellular injury contexts have reported rapid translocation of ANXA4 to the plasma and nuclear membranes in a Ca^{2+}-dependent manner (Piljic & Schultz, 2006; Skrahina et al., 2008). Therefore, we began by testing whether ANXA4 is responsive to mechanical membrane injury on a similar rapid time scale. Expression of ANXA4-GFP was induced by transient transfection of A7 cells, an astrocytic cell line derived from rat optic nerve (Exler et al., 2016; Geller & Dubois-Dalcq, 1988), and confirmed by western blot analysis lysates for ANXA4 (Supporting Information: Figure 1A). The response of ANXA4-GFP to Ca^{2+} elevation was confirmed by treating transfected cells with 10 μM of the calcium ionophore, ionomycin, for 5 min. Ionomycin treatment caused ANXA4-GFP to rapidly redistribute to nuclear and plasma membranes (Supporting Information: Figure 1B), as previously reported (Piljic & Schultz, 2006). Following this validation, we applied direct mechanical membrane injury using glass beads or needle scratch assays, and then immediately fixed for imaging. In uninjured cells ANXA4-GFP was distributed uniformly, but either glass bead or scratch injury also caused a rapid redistribution of ANXA4-GFP to the plasma and nuclear membranes (Figure 1a).

Based on these results, we wondered whether a similar translocation could be induced by mechanical stretch? Therefore, ANXA4-GFP transfected cells were also exposed to 12% equiaxial cyclic stretch injury, which we have previously used to model strains experienced by astrocytes in the lamina cribrosa under glaucomatous conditions (Exler et al., 2016; R. Rogers et al., 2012; R. S. Rogers et al., 2012). Stretched cells exhibited a rapid translocation of GFP signal after 5 min of stretching (Figure 1a). To confirm this observation, stretched and control cells were also immunostained for endogenous ANXA4 protein. In control cells the ANXA4 signal was faint and diffuse throughout cells. However, following 5 min of stretch the ANXA4 staining was stronger and localized to membrane structures, consistent with the ANXA4-GFP signal (Figure 1b). Collectively, these results suggest that ANXA4 responds to direct and stretch-induced damage by redistributing along membrane structures.

3.2 | Increased membrane permeability is induced following biomechanical strain in a calcium-dependent manner

Given the proposed roles of ANXA4 in PMR, we investigated if membrane damage can occur during pathologically relevant biomechanical strain. FM 1–43 is a water-soluble dye that has been extensively used in studies involving the plasma membrane integrity and dynamics (Beckwith et al., 2020; Bouter et al., 2011; A. K. McNeil et al., 2006). The dye is impermeable to intact lipid membranes, but becomes fluorescent when passively inserted

into damaged membrane edges. As an initial test A7 cells were incubated in FM 1–43 dye and subjected to a scratch injury followed by immediate fixation and imaging. In each well most of the cells in the field exhibited no fluorescence with FM 1–43 dye, indicating no permeability under homeostatic conditions. However, cells that lay directly along the scratch line brightly fluoresced around the damaged membranes (Figure 1c). This approach was then applied to A7 cells undergoing 12% mechanical stretch for 5 min in the presence of FM 1–43. As previously, no injury resulted in minimal fluorescence. However, robustly increased fluorescence was observed after stretch under conditions that included Ca^{2+} (Figure 1d). As extracellular calcium can facilitate PMR protein activity, we also examined FM 1–43 fluorescence of cells stretched in Ca^{2+}-free media and observed a significantly stronger signal (Figure 1d). Mean fluorescence intensity analysis of these experiments revealed significantly higher staining in stretched cells than control, and without Ca^{2+} compared to with Ca^{2+} (Figure 1e). These data are consistent with rapidly compromised membrane permeability following biomechanical stretch that is partially Ca^{2+}-dependent.

3.3 | ANXA4 is required for efficient membrane repair during biomechanical stretch

As a second method for verifying our stretched membrane permeability results, we tested an alternative membrane impermeable dye, DRAQ7, which fluoresces upon cell entry following membrane compromise and DNA binding (Beckwith et al., 2020). DRAQ7 was added to stretched and nonstretched control cells as previously, and assessed for the resulting nuclear fluorescence. Similar to previous experiments with FM 1–43FX, there was little DRAQ7 dye incorporation under control conditions. However, following stretch insult cells were 10-fold more permeable to DRAQ7 influx than nonstretch controls (Figure 2a,b). This experiment provides an independent validation of stretch-induced membrane permeability.

To examine whether ANXA4 impacts membrane permeability during stretch, ANXA4 was knocked down and plasma membrane permeability was assessed. We found that the DRAQ7 dye provided a better signal-to-noise ratio when combined with siRNA transfections than FM 1–43FX, and this method was chosen for knockdown experiments. Transient knockdown of endogenous ANXA4 was induced by siRNA-mediated gene silencing and was compared to a scrambled NT siRNA control. Efficient protein knockdown and detection was confirmed through western blot and densitometry (Figure 2c, Supporting Information: Figure 3). Following knockdown, cells were incubated with DRAQ7 and stretched. There was no significant change in DRAQ7 staining under nonstretch control conditions following ANXA4 knockdown compared to NT (Figure 2d,e). In comparison, stretch insult dramatically increased DRAQ7 staining for both groups. However, cells stretched with reduced ANXA4 displayed significantly increased DRAQ7 fluorescence compared to stretched NT control (Figure 2d,e). This result indicates greater membrane permeability in cells lacking ANXA4 under biomechanical stretch conditions.

3.4 | Recombinant ANXA4 can partially rescue compromised membranes following mechanical strain

Given the membrane localization of activated ANXA4, and the hypothesized roles of the annexin family in PMR, we sought to test whether additional ANXA4 is able to reduce membrane compromise following mechanical stretch. Since transfection protocols

introduced membrane damage that increased baseline dye incorporation, we sought an alternative gain of function method. Based on evidence that exogenous soluble ANXA5 is able to infiltrate damage cites to improve repair in mouse perivascular cells following laser injury (Bouter et al., 2011), we tested whether recombinant ANXA4 is similarly able to reduce membrane compromise following mechanical stretch. Purified recombinant human ANXA4 was generated in a bacterial expression system (Supporting Information: Figure 2), and added at two concentrations to A7 cells followed immediately by 12% stretch for 5 min, in the presence of FM 1–43FX. Either 5 or 50 μg/ml recombinant ANXA4 (rANXA4) appeared to reduce stretch-induced fluorescence compared to vehicle (Figure 3a). Fluorescence intensity analyses showed that in the presence of Ca^{2+}, FM 1–43FX signal is significantly reduced following treatment with either 5 or 50 μg/ml of rANXA4 compared to vehicle (Figure 3b). However, in the absence of Ca^{2+}, only the higher 50 μg/ml concentration significantly attenuated the FM 1–43FX signal (Figure 3c), consistent with a role for extracellular Ca^{2+} in this mechanism.

These rapid cell membrane permeability studies were technically challenging to perform and analyze. Therefore, most of this study was undertaken in the well-characterized A7 astrocyte cell line. To confirm the results in more relevant primary cells, we repeated the experiment with rANXA4 treatment of human ONH astrocytes that were exposed to stretch in Ca^{2+}-free media. Similar to the A7 cells, FM1–43 signal was significantly increased in human ONH astrocytes following exposure to 12% stretch for 5 min (Figure 3d,e). This increase was reduced with treatment of 50 μg/ml rANXA4 (Figure 3d,e). Thus, rANXA4 was able to partially rescue stretch-induced membrane compromise in A7 cells and human ONH astrocytes.

3.5 | ANXA4 colocalizes near actin along cell junctions during membrane damage

The interactions involved in ANXA4 membrane activities remain unclear. Other members of the annexin family form membrane scaffolds when activated that interact with cytoskeletal components, particularly F-actin (Jaiswal et al., 2014). However, such an interaction has not yet been well described for ANXA4. Therefore, we assessed this possibility in relation to mechanical stretch. In colocalization studies, only diffuse ANXA4 staining was observed under control conditions. Yet, after 5 min of stretch, the membrane-localized ANXA4 was aligned with cell junctions and robustly colocalized with, or was closely adjacent, to cortical F-actin (Figure 4a, Supporting Information: Figure 4). Notably, similar colocalization was also observed with ANXA4 and F-actin at focal damage sites following glass bead injury (Supporting Information: Figure 5).

To test for interaction between this association during biomechanical injury, A7 cells were treated with disruptors of actin dynamics; cytocholasin D (an actin polymerization inhibitor), or jasplakinolide (an actin stabilizer). Disruptors were applied to the cells for 30 min before 5 min stretch with FM 1–43FX as previously. Treated stretch cells were co-stained for ANXA4 to observe how its localization responded to disrupted actin. Exposure to either cytochalasin D or jasplakinolide severely disrupted F-actin staining during this brief period, and also caused a corresponding and colocalized disruption in ANXA4 staining (Figure 4b). Interestingly, neither cytochalasin D or jasplakinolide treated cells showed

a significant increase in FM 1–43FX fluorescence compared to vehicle in control cells, suggesting their membranes remained intact (Supporting Information: Figure 6). However, there was modestly increased FM 1–43FX fluorescence intensity compared to vehicle for each compound in the context of stretch, indicating increased membrane permeability (Supporting Information: Figure 6). Finally, cell sections were imaged by TEM to directly visualize membranes and junctions following stretch. At high magnification tight junctions could be clearly observed between cell contacts, but after stretch many of these junctions appeared open or torn (Figure 4c). Additionally, anti-ANXA4 immunogold labeling was also performed on TEM samples. We found the preparation of and labeling steps challenging to optimize on the Bioflex plate membranes. However, high magnification identified anti-ANXA4 gold particles localized near cell plasma membranes in stretch samples, but not in no-primary controls (Figure 4d, Supporting Information: Figure 4). Taken together, these results suggest that activated ANXA4 may interact with cortical F-actin at cell junctions in response to plasma membrane injury.

3.6 | ANXA4 colocalizes near F-actin in the ONH in vivo

To demonstrate ANXA4 interactions with cytoskeletal components in vivo, rat ONH tissues were sectioned and stained with ANXA4 and a variety of markers. ONH cross-sections imaged at high magnification revealed colocalization of ANXA4 and actin in a lattice surrounding β3-tubulin positive nerve fiber bundles (Figure 4e). This overlap was quantified and confirmed by measuring the colocalization coefficient of ANXA4 with F-actin, GFAP, or β3-tubulin across multiple images confirming the strongest colocalization with actin (Figure 4f). Similarly, longitudinal sections of the ONH show strong colocalization with ANXA4 and F-actin, but not with β3 tubulin or the intermediate filament GFAP (Supporting Information: Figure 7). Interestingly, this colocalization was preserved during actin realignment in vivo following acute IOP injury (Supporting Information: Figure 8), similar to changes noted previously by Tehrani et al (2014).

3.7 | ANXA4 colocalizes near F-actin in the human ONH and displays altered localization in glaucomatous tissues

The human ONH exhibits unique anatomic and structural features compared to the rodent eye. In particular, the lamina cribrosa (LCr) is a collagenous mesh that provides biomechanical support to RGC nerve fibers in combination with neighboring astrocytes (Sigal et al., 2007). Previous work has reported the increased presence of cross-linked actin networks (CLANS) in the glaucomatous LCr in association with the biomechanical strain experienced by these tissues (Bermudez et al., 2017; Job et al., 2010). To test whether altered ANXA4 localization is also present in the human ONH, control and pathological sections underwent antigen retrieval and were stained with antibodies to ANXA4. Parallel sections were incubated with no-primary antibody controls, and a competition experiment with rANXA4 confirmed the specificity of the staining signal (Supporting Information: Figure 4). Sections were costained with phalloidin to observe any changes in actin fiber organization.

In healthy eyes the ANXA4-phalloidin staining was closely colocalized, and was particularly prominent in the LCr region (Figure 5a). More detail was evident at high

magnification, where constitutive ANXA4 and actin signals were relatively low and localized to cell junctions organized along laminar beams (Figure 5b). In marked contrast, staining of age-matched ONH samples from glaucoma patients consistently showed clear foci of ANXA4 and actin colocalizations throughout the LCr region, which also displayed a general structural disorganization. These foci became very clear when viewed as a merged image at high magnification, as they highlighted as bright yellow punctae (Figure 5b). Note, no substantive ANXA4 staining or autofluorescence was observed in controls without primary antibody at these settings (Supporting Information: Figure 4). In addition, close inspection of the ANXA4 signal at high magnification indicated increased membrane localization in the glaucomatous LCr, including both cell and nuclear membrane staining (Figure 5c). This localization is reminiscent of the images from cells exposed to stretch injury (Figure 1). Quantification of ANXA4:actin foci across multiple control and glaucomatous eyes indicates a highly significant correlation with the disease samples ($p < 0.0001$) (Figure 5d). The altered localization of ANXA4 in the glaucomatous human LCr is consistent with our in vitro observations associated with membrane injury and biomechanical stretch injury.

4 | DISCUSSION

Annexins represent a fairly ubiquitous protein family with members implicated in essential cellular functions linking calcium to membrane and cytoskeletal dynamics (Gerke et al., 2005; Hayes et al., 2004). Family members have been broadly reported to be upregulated in a variety of neurodegenerative pathologies, including glaucoma, traumatic and ischemic injury, and Alzheimer's disease (Dias & Nylandsted, 2021; Facio et al., 2011; Johnson et al., 2007; Ries et al., 2021; R. Rogers et al., 2012; R. S. Rogers et al., 2012; Ruan et al., 2013; Yap et al., 2018). Upon elevation of intracellular calcium, ANXA4 translocates to membranes where it forms lateral assemblies of 2D trimers (Newman et al., 1991). This crystalline structure arrangement has been shown to affect membrane properties including rigidity, fluidity, and lipid domain stabilization, to affect permeability and repair (Creutz et al., 2012; Piljic & Schultz, 2006; Skrahina et al., 2008). In the context of thermal injury and hypo-osmotic swelling ANXA4 has been demonstrated to direct membrane curvature at the wound edge, working with ANXA6 to direct constriction and closure (Boye et al., 2017). These data have been supported by recent reports similarly linking ANXA4 function to sense and induce membrane curvature during PMR (Boye et al., 2017; Florentsen et al., 2021; Mularski et al., 2021). However, the role of ANXA4 in biomechanical strain has remained less clear. Our results suggest that relatively mild pathologically relevant equiaxial stretch compromises membrane integrity and results in ANXA4 translocation to participate in a PMR in a manner that is partially dependent on extracellular calcium. Furthermore, loss-of-function studies show that ANXA4 activity is partially required to efficiently modulate repair of this injury. Also, exogenous rANXA4 is able to reduce membrane compromise, similar to that observed with soluble ANXA5 (Bouter et al., 2011). However, additional studies will be needed to further dissect the function of endogenous ANXA4, and to explore how multiple annexins with overlapping and distinct roles in PMR mechanics may partially compensate for altered ANXA4 function in this context.

Our results also implicate interactions between ANXA4 and actin in these dynamics in vitro, and in the retina in vivo, showing strain-induced colocalizations at the membrane that is concentrated at cell junctions. We note that the colocalization between the two proteins is not always a perfect overlap, and it sometimes appears the ANXA4 and actin signals lie very closely alongside each other. The cortical actin cytoskeleton is in intimate contact with the plasma membrane and is a fundamental regulator of PMR (Abreu-Blanco et al., 2011; Bement et al., 1999). Tight tethering of cortical actin to the membrane can increase membrane tension and inhibit passive resealing after injury (Togo et al., 2000). Following injury, it is important for actin to quickly depolymerize at the wound site to release membrane tension so the wounded edges can subsequently be brought together (Abreu-Blanco et al., 2011). This is then followed by rapid actin repolymerization. Laser injury induces calcium-dependent membrane recruitment of Annexin 2 to help reseal plasma membranes by facilitating rapid F-actin polymerization (Jaiswal et al., 2014) and we propose a related function for ANXA4 in the context of biomechanical strain.

Biomechanical strain and cytoskeletal remodeling of ONH astrocytes and LCr cells are cardinal features of glaucoma; a neurodegenerative disorder in which vision degrades due to the gradual and irreversible loss of retinal ganglion cells (RGCs) (Alqawlaq et al., 2019; Boal et al., 2021; Garcia-Bermudez et al., 2021). Glaucomatous pathology is closely associated with age and elevated intraocular pressure that translates into biomechanical insult at the ONH, believed to be a principal site of early RGC axonal damage (Alqawlaq et al., 2019; Mathew et al., 2021; Nguyen & Ethier, 2015; Stowell et al., 2017). IOP-induced strain is proposed to exert mechanical damage on glia and axons at the ONH, generate microischemic/reperfusion conditions, and elevated Ca^{2+} dynamics and MAPK signaling cascades that can induce apoptosis (Alqawlaq et al., 2019; Exler et al., 2016; Nahirnyj et al., 2013). At the same time, age-induced lipid peroxidation results in increased cell membrane rigidity, thinning, and permeability, leaving cells vulnerable to biomechanical injury (Catala & Diaz, 2016; Naudi et al., 2013). Measurements and modeling of strain during experimental IOP elevation show that the LCr tissue suffers substantial and abnormal levels of tissue distortion (Bellezza et al., 2000; Downs, 2015; Norman et al., 2011; Sigal et al., 2014). This unique structure composed of collagen fibers and astrocytic processes is believed to provide mechanical support to the delicate RGC nerve fibers. Based on observed tissue deformations, anatomical computational modeling has predicted stretch and other strains at the ONH in the LCr of eyes that experienced elevation of IOPs up to 50 mmHg in the range of 5%–15% (Beotra et al., 2018; Sigal et al., 2004, 2007), which are consistent with the 12% value used for the present studies. Notably, recent microstructural modeling also suggests that much higher strains can be experienced at specific sites on LCr pore beams (Voorhees et al., 2017). However, the molecular mechanisms connecting this strain to the resulting tissue damage have remained elusive.

To our knowledge, cell membrane integrity and permeability have not previously been assessed in the context of glaucomatous biomechanical insult. However, in the CNS transient membrane tearing (mechanoporation) has been linked to traumatic brain injury (Hemphill et al., 2015; Hernandez et al., 2019), and cytotoxic pores formed by protein aggregates have been linked to Alzheimer's and Parkinson's diseases (Bharadwaj et al., 2018; Bode et al., 2019; Fecchio et al., 2013; Reynolds et al., 2011; Shrivastava et al., 2017),

suggesting that cell membrane integrity may be a common thread in neurodegenerative mechanisms. Based on the results presented here, we propose a new model in which pathological biomechanical insult due to increased IOP and age can result in microstructural membrane damage that generates transient increases in localized calcium dynamics. This extracellular calcium signal could activate ANXA4 and actin remodeling components of the PMR response (Figure 5e). Rapidly increased calcium concentrations have been previously reported in Fura-2/AM-loaded human LCr cells undergoing 15% mechanical insult (Quill et al., 2015). Notably, this gradual increase was observed even in the presence of the calcium channel blocker verapamil, suggesting alternative routes of calcium entry. In addition, elevated intracellular calcium following scratch injury can activate GFAP expression in astrocytes and lead to astrogliosis (Gao et al., 2013). Likewise, cytoskeletal changes in astrocytes following IOP-induced strain have been linked to altered Ca^{2+} signaling, and disrupted axonal transport, and mechanical support (Tehrani et al., 2014). Formation of cross-linked actin networks (CLANs) have also been reported in glaucomatous LCr cells, both in culture and in situ (Bermudez et al., 2017; Job et al., 2010). However, limitations in imaging resolution following antigen retrieval prevented us from definitively linking the ANXA4:actin foci we observed in tissues with the canonical hub and spoke CLAN structures, and the staining may represent a distinct degenerative feature.

There have been limited studies on the functions of annexin proteins following IOP-induced injury, although altered expression or localization of family members have been identified by ourselves and others (Johnson et al., 2007; R. S. Rogers et al., 2012; Yap et al., 2018). In particular, the membrane binding properties of annexin V in apoptosing RGCs have been successfully exploited to image dying neurons in vivo, and in the clinic (Cordeiro et al., 2017; Yap et al., 2018). Our data suggests ANXA4 activation may be a disease biomarker in the LCr, and is capable of integrating localized membrane microinjury with extrinsic Ca^{2+} signaling and cytoskeletal remodeling. This model suggests a novel mechanism that requires no additional specialized membrane mechanosensor to initiate Ca^{2+}-driven cellular responses to IOP-induced biomechanical strain. A variety of annexins are commonly reported to be upregulated in models of disease that experience chronic biomechanical insult, such as glaucoma, muscular dystrophy, and cardiovascular disease (Cagliani et al., 2005; Holland et al., 2013; Johnson et al., 2007; La et al., 2001; Monastyrskaya et al., 2009; R. S. Rogers et al., 2012; Waddell et al., 2011). Therefore, the link between moderate biomechanical strain and PMR mechanisms may be relevant to a variety of chronic injury and disease mechanisms. Future studies will be needed to elaborate roles on mechanically altered membrane permeability in the context of these chronic degenerative injuries.

Supplementary Material

Refer to Web version on PubMed Central for supplementary material.

ACKNOWLEDGMENTS

The authors would like to thank Ali Darbandi, Lindsey Fiddes, and Yan Chen for help with EM imaging and Izhar Livne-Bar for comments on the manuscript. This study was supported by NSERC grant RGPIN-2015-06561 (JMS), CIHR grants MOP123448 (JMS, JGF and IAS) and PJT166201 (JMS), and NIH grant 5RO1EY026082 (JMS and JGF), and a pilot grant from GRSC. NV received a VSRP fellowship. JMS holds the TWGH Foundation Glaucoma Research Chair.

Funding information

Natural Sciences and Engineering Research Council of Canada, Grant/Award Number: RGPIN-2015-06561; Canadian Institutes of Health Research, Grant/Award Numbers: MOP123448, PJT166201; Glaucoma Research Society of Canada, Grant/Award Number: Pilot Grant; National Institutes of Health, Grant/Award Number: 5R01EY026082

REFERENCES

Abreu-Blanco MT, Verboon JM, & Parkhurst SM (2011). Cell wound repair in Drosophila occurs through three distinct phases of membrane and cytoskeletal remodeling. Journal of Cell Biology, 193(3), 455–464. 10.1083/jcb.201011018 [PubMed: 21518790]

Almasieh M, Wilson AM, Morquette B, Cueva Vargas JL, & Di Polo A (2012). The molecular basis of retinal ganglion cell death in glaucoma. Progress in Retinal and Eye Research, 31(2), 152–181. 10.1016/j.preteyeres.2011.11.002 [PubMed: 22155051]

Alqawlaq S, Flanagan JG, & Sivak JM (2019). All roads lead to glaucoma: Induced retinal injury cascades contribute to a common neurodegenerative outcome. Experimental Eye Research, 183, 88–97. 10.1016/j.exer.2018.11.005 [PubMed: 30447198]

Alqawlaq S, Livne-Bar I, Williams D, D'Ercole J, Leung SW, Chan D, Tuccitto A, Datti A, Wrana JL, Corbett AH, Schmitt-Ulms G, & Sivak JM (2020). An endogenous PI3K interactome promoting astrocyte-mediated neuroprotection identifies a novel association with RNA binding protein ZC3H14. Journal of Biological Chemistry, 296, 100118. 10.1074/jbc.RA120.015389 [PubMed: 33234594]

Beckwith KS, Beckwith MS, Ullmann S, Sætra RS, Kim H, Marstad A, Åsberg SE, Strand TA, Haug M, Niederweis M, Stenmark HA, & Flo TH (2020). Plasma membrane damage causes NLRP3 activation and pyroptosis during *Mycobacterium tuberculosis* infection. Nature Communications, 11(1), 2270. 10.1038/s41467-020-16143-6

Bellezza AJ, Hart RT, & Burgoyne CF (2000). The optic nerve head as a biomechanical structure: Initial finite element modeling. Investigative Ophthalmology & Visual Science, 41(10), 2991–3000. [PubMed: 10967056]

Bement WM, Mandato CA, & Kirsch MN (1999). Wound-induced assembly and closure of an actomyosin purse string in Xenopus oocytes. Current Biology, 9(11), 579–587. 10.1016/s0960-9822(99)80261-9 [PubMed: 10359696]

Beotra MR, Wang X, Tun TA, Zhang L, Baskaran M, Aung T, Strouthidis NG, & Girard M (2018). In vivo three-dimensional lamina cribrosa strains in healthy, ocular hypertensive, and glaucoma eyes following acute intraocular pressure elevation. Investigative Ophthalmology & Visual Science, 59(1), 260–272. 10.1167/iovs.17-21982 [PubMed: 29340640]

Bermudez JY, Montecchi-Palmer M, Mao W, & Clark AF (2017). Cross-linked actin networks (CLANs) in glaucoma. Experimental Eye Research, 159, 16–22. 10.1016/j.exer.2017.02.010 [PubMed: 28238754]

Bharadwaj P, Solomon T, Malajczuk CJ, Mancera RL, Howard M, Arrigan D, Newsholme P, & Martins RN (2018). Role of the cell membrane interface in modulating production and uptake of Alzheimer's beta amyloid protein. Biochimica et Biophysica Acta, 1860(9), 1639–1651. 10.1016/j.bbamem.2018.03.015 [PubMed: 29572033]

Boal AM, Risner ML, Cooper ML, Wareham LK, & Calkins DJ (2021). Astrocyte networks as therapeutic targets in glaucomatous neurodegeneration. Cells, 10(6), 1368. 10.3390/cells10061368 [PubMed: 34199470]

Bode DC, Freeley M, Nield J, Palma M, & Viles JH (2019). Amyloid-beta oligomers have a profound detergent-like effect on lipid membrane bilayers, imaged by atomic force and electron microscopy. Journal of Biological Chemistry, 294(19), 7566–7572. 10.1074/jbc.AC118.007195 [PubMed: 30948512]

Bouter A, Gounou C, Bérat R, Tan S, Gallois B, Granier T, D'estaintot BL, Pöschl E, Brachvogel B, & Brisson AR (2011). Annexin-A5 assembled into two-dimensional arrays promotes cell membrane repair. Nature Communications, 2, 270. 10.1038/ncomms1270

Boye TL, Maeda K, Pezeshkian W, Sønder SL, Haeger SC, Gerke V, Simonsen AC, & Nylandsted J (2017). Annexin A4 and A6 induce membrane curvature and constriction during cell membrane repair. Nature Communications, 8(1), 1623. 10.1038/s41467-017-01743-6

Bubb MR, Senderowicz AM, Sausville EA, Duncan KL, & Korn ED (1994). Jasplakinolide, a cytotoxic natural product, induces actin polymerization and competitively inhibits the binding of phalloidin to F-actin. Journal of Biological Chemistry, 269(21), 14869–14871. [PubMed: 8195116]

Burgoyne CF (2011). A biomechanical paradigm for axonal insult within the optic nerve head in aging and glaucoma. Experimental Eye Research, 93(2), 120–132. 10.1016/j.exer.2010.09.005 [PubMed: 20849846]

Cagliani R, Magri F, Toscano A, Merlini L, Fortunato F, Lamperti C, Rodolico C, Prelle A, Sironi M, Aguennouz M, Ciscato P, Uncini A, Moggio M, Bresolin N, & Comi GP (2005). Mutation finding in patients with dysferlin deficiency and role of the dysferlin interacting proteins annexin A1 and A2 in muscular dystrophies. Human Mutation, 26(3), 283. 10.1002/humu.9364

Catala A, & Diaz M (2016). Editorial: Impact of lipid peroxidation on the physiology and pathophysiology of cell membranes. Frontiers in Physiology, 7, 423. 10.3389/fphys.2016.00423 [PubMed: 27713704]

Cordeiro MF, Normando EM, Cardoso MJ, Miodragovic S, Jeylani S, Davis BM, Guo L, Ourselin S, A'Hern R, & Bloom PA (2017). Real-time imaging of single neuronal cell apoptosis in patients with glaucoma. Brain, 140(6), 1757–1767. 10.1093/brain/awx088 [PubMed: 28449038]

Crawford Downs J, Roberts MD, & Sigal IA (2011). Glaucomatous cupping of the lamina cribrosa: A review of the evidence for active progressive remodeling as a mechanism. Experimental Eye Research, 93(2), 133–140. 10.1016/j.exer.2010.08.004 [PubMed: 20708001]

Creutz CE, Hira JK, Gee VE, & Eaton JM (2012). Protection of the membrane permeability barrier by annexins. Biochemistry, 51(50), 9966–9983. 10.1021/bi3013559 [PubMed: 23190562]

Dias C, & Nylandsted J (2021). Plasma membrane integrity in health and disease: Significance and therapeutic potential. Cell Discovery, 7(1), 4. 10.1038/s41421-020-00233-2 [PubMed: 33462191]

Downs JC (2015). Optic nerve head biomechanics in aging and disease. Experimental Eye Research, 133, 19–29. 10.1016/j.exer.2015.02.011 [PubMed: 25819451]

Draeger A, Monastyrskaya K, & Babiychuk EB (2011). Plasma membrane repair and cellular damage control: The annexin survival kit. Biochemical Pharmacology, 81(6), 703–712. 10.1016/j.bcp.2010.12.027 [PubMed: 21219882]

Eberhard DA, Brown MD, & VandenBerg SR (1994). Alterations of annexin expression in pathological neuronal and glial reactions. Immunohistochemical localization of annexins I, II (p36 and p11 subunits), IV, and VI in the human hippocampus. The American Journal of Pathology, 145(3), 640–649. [PubMed: 8080046]

Exler RE, Guo X, Chan D, Livne-Bar I, Vicic N, Flanagan JG, & Sivak JM (2016). Biomechanical insult switches PEA-15 activity to uncouple its anti-apoptotic function and promote erk-mediated tissue remodeling. Experimental Cell Research, 340(2), 283–294. 10.1016/j.yexcr.2015.11.023 [PubMed: 26615958]

Facio FN Jr., Sena AA, Araújo LP, Mendes GE, Castro I, Luz MA, Yu SM, Oliani EA, & Burdmann L (2011). Annexin 1 mimetic peptide protects against renal ischemia/reperfusion injury in rats. Journal of Molecular Medicine (Berl), 89(1), 51–63. 10.1007/s00109-010-0684-4

Fecchio C, De Franceschi G, Relini A, Greggio E, Dalla Serra M, Bubacco L, & Polverino de Laureto P (2013). alpha-synuclein oligomers induced by docosahexaenoic acid affect membrane integrity. PLoS One, 8(11), e82732. 10.1371/journal.pone.0082732 [PubMed: 24312431]

Florentsen CD, Kamp-Sonne A, Moreno-Pescador G, Pezeshkian W,Hakami Zanjani AA, Khandelia H, Nylandsted J, & Bendix PM (2021). Annexin A4 trimers are recruited by high membrane curvatures in giant plasma membrane vesicles. Soft Matter, 17(2), 308–318. 10.1039/d0sm00241k [PubMed: 32756654]

Gao K, Wang CR, Jiang F, Wong AY, Su N, Jiang JH, Chai RC, Vatcher G, Teng J, Chen J, Jiang YW, & Yu AC (2013). Traumatic scratch injury in astrocytes triggers calcium influx to activate the JNK/c-Jun/AP-1 pathway and switch on GFAP expression. Glia, 61(12), 2063–2077. 10.1002/glia.22577 [PubMed: 24123203]

Garcia-Bermudez MY, Freude KK, Mouhammad ZA, van Wijngaarden P, Martin KK, & Kolko M (2021). Glial cells in glaucoma: Friends, foes, and potential therapeutic targets. Frontiers of Neurology, 12, 624983. 10.3389/fneur.2021.624983

Geller HM, & Dubois-Dalcq M (1988). Antigenic and functional characterization of a rat central nervous system-derived cell line immortalized by a retroviral vector. Journal of Cell Biology, 107(5), 1977–1986. [PubMed: 3053737]

Gerke V, Creutz CE, & Moss SE (2005). Annexins: Linking Ca2+ signalling to membrane dynamics. Nature Reviews Molecular Cell Biology, 6(6), 449–461. 10.1038/nrm1661 [PubMed: 15928709]

Gerke V, & Moss SE (2002). Annexins: From structure to function. Physiological Reviews, 82(2), 331–371. 10.1152/physrev.00030.2001 [PubMed: 11917092]

Guo X, Jiang Q, Tuccitto A, Chan D, Alqawlaq S, Won GJ, & Sivak JM (2018). The AMPK-PGC-1alpha signaling axis regulates the astrocyte glutathione system to protect against oxidative and metabolic injury. Neurobiology of Disease, 113, 59–69. 10.1016/j.nbd.2018.02.004 [PubMed: 29438738]

Hayes MJ, Rescher U, Gerke V, & Moss SE (2004). Annexin-actin interactions. Traffic, 5(8), 571–576. 10.1111/j.1600-0854.2004.00210.x [PubMed: 15260827]

Hemphill MA, Dauth S, Yu CJ, Dabiri BE, & Parker KK (2015). Traumatic brain injury and the neuronal microenvironment: A potential role for neuropathological mechanotransduction. Neuron, 85(6), 1177–1192. 10.1016/j.neuron.2015.02.041 [PubMed: 25789754]

Hernandez ML, Chatlos T, Gorse KM, & Lafrenaye AD (2019). Neuronal membrane disruption occurs late following diffuse brain trauma in rats and involves a subpopulation of NeuN negative cortical neurons. Frontiers of Neurology and Neuroscience, 10, 1238. 10.3389/fneur.2019.01238

Holland A, Dowling P, Zweyer M, Swandulla D, Henry M, Clynes M, & Ohlendieck K (2013). Proteomic profiling of cardiomyopathic tissue from the aged mdx model of Duchenne muscular dystrophy reveals a drastic decrease in laminin, nidogen and annexin. Proteomics, 13(15), 2312–2323. 10.1002/pmic.201200578 [PubMed: 23713012]

Horn A, & Jaiswal JK (2018). Cellular mechanisms and signals that coordinate plasma membrane repair. Cellular and Molecular Life Sciences, 75(20), 3751–3770. 10.1007/s00018-018-2888-7 [PubMed: 30051163]

Jaiswal JK, Lauritzen SP, Scheffer L, Sakaguchi M, Bunkenborg J, Simon SM, Kallunki T, Jäättelä M, & Nylandsted J (2014). S100A11 is required for efficient plasma membrane repair and survival of invasive cancer cells. Nature Communications, 5, 3795. 10.1038/ncomms4795

Job R, Raja V, Grierson I, Currie L, O'Reilly S, Pollock N, Knight E, & Clark AF (2010). Cross-linked actin networks (CLANs) are present in lamina cribrosa cells. British Journal of Ophthalmology, 94(10), 1388–1392. 10.1136/bjo.2009.176032 [PubMed: 20693558]

Johnson EC, Jia L, Cepurna WO, Doser TA, & Morrison JC (2007). Global changes in optic nerve head gene expression after exposure to elevated intraocular pressure in a rat glaucoma model. Investigative Ophthalmology & Visual Science, 48(7), 3161–3177. 10.1167/iovs.06-1282 [PubMed: 17591886]

Kulik L, Fleming SD, Moratz C, Reuter JW, Novikov A, Chen K, Andrews KA, Markaryan A, Quigg RJ, Silverman GJ, Tsokos GC, & Holers VM (2009). Pathogenic natural antibodies recognizing annexin IV are required to develop intestinal ischemia-reperfusion injury. Journal of Immunology, 182(9), 5363–5373. 10.4049/jimmunol.0803980

La M, D'Amico M, Bandiera S, Di Filippo C, Oliani SM, Gavins FN, Flower RJ, & Perretti M (2001). Annexin 1 peptides protect against experimental myocardial ischemia-reperfusion: Analysis of their mechanism of action. FASEB Journal, 15(12), 2247–2256. 10.1096/fj.01-0196com [PubMed: 11641252]

Liu YY, Ge C, Tian H, Jiang JY, Zhao FY, Li H, Chen TY, Yao M, & Li JJ (2017). The transcription factor Ikaros inhibits cell proliferation by downregulating ANXA4 expression in hepatocellular carcinoma. American Journal of Cancer Research, 7(6), 1285–1297. [PubMed: 28670491]

Livne-Bar I, Lam S, Chan D, Guo X, Askar I, Nahirnyj A, Flanagan JG, & Sivak JM (2016). Pharmacologic inhibition of reactive gliosis blocks TNF-alpha-mediated neuronal apoptosis. Cell Death and Disease, 7(9), e2386. 10.1038/cddis.2016.277 [PubMed: 27685630]

Livne-Bar I, Wei J, Liu HH, Alqawlaq S, Won GJ, Tuccitto A, Gronert K, Flanagan JG, & Sivak JM (2017). Astrocyte-derived lipoxins A4 and B4 promote neuroprotection from acute and chronic injury. Journal of Clinical Investigation, 127(12), 4403–4414. 10.1172/JCI77398 [PubMed: 29106385]

Mathew DJ, Livne-Bar I, & Sivak JM (2021). An inducible rodent glaucoma model that exhibits gradual sustained increase in intraocular pressure with distinct inner retina and optic nerve inflammation. Scientific Reports, 11(1), 22880. 10.1038/s41598-021-02057-w [PubMed: 34819548]

McNeil AK, Rescher U, Gerke V, & McNeil PL (2006). Requirement for annexin A1 in plasma membrane repair. Journal of Biological Chemistry, 281(46), 35202–35207. 10.1074/jbc.M606406200 [PubMed: 16984915]

McNeil PL, & Kirchhausen T (2005). An emergency response team for membrane repair. Nature Reviews Molecular Cell Biology, 6(6), 499–505. 10.1038/nrm1665 [PubMed: 15928713]

McNeil PL, & Steinhardt RA (2003). Plasma membrane disruption: Repair, prevention, adaptation. Annual Review of Cell and Developmental Biology, 19, 697–731. 10.1146/annurev.cellbio.19.111301.140101

Monastyrskaya K, Babiychuk EB, & Draeger A (2009). The annexins: Spatial and temporal coordination of signaling events during cellular stress. Cellular and Molecular Life Sciences, 66(16), 2623–2642. 10.1007/s00018-009-0027-1 [PubMed: 19381436]

Mularski A, Sonder SL, Heitmann ASB, Nylandsted J, & Simonsen AC (2021). Simultaneous membrane binding of Annexin A4 and A5 suppresses 2D lattice formation while maintaining curvature induction. Journal of Colloid and Interface Science, 600, 854–864. 10.1016/j.jcis.2021.05.067 [PubMed: 34052534]

Nahirnyj A, Livne-Bar I, Guo X, & Sivak JM (2013). ROS detoxification and proinflammatory cytokines are linked by p38 MAPK signaling in a model of mature astrocyte activation. PLoS One, 8(12), e83049. 10.1371/journal.pone.0083049 [PubMed: 24376630]

Naudi A, Jove M, Ayala V, Portero-Otin M, Barja G, & Pamplona R (2013). Membrane lipid unsaturation as physiological adaptation to animal longevity. Frontiers in Physiology, 4, 372. 10.3389/fphys.2013.00372 [PubMed: 24381560]

Newman RH, Leonard K, & Crumpton MJ (1991). 2D crystal forms of annexin IV on lipid monolayers. FEBS Letters, 279(1), 21–24. 10.1016/0014-5793(91)80240-4 [PubMed: 1825300]

Nguyen TD, & Ethier CR (2015). Biomechanical assessment in models of glaucomatous optic neuropathy. Experimental Eye Research, 141, 125–138. 10.1016/j.exer.2015.05.024 [PubMed: 26115620]

Norman RE, Flanagan JG, Sigal IA, Rausch SM, Tertinegg I, & Ethier CR (2011). Finite element modeling of the human sclera: Influence on optic nerve head biomechanics and connections with glaucoma. Experimental Eye Research, 93(1), 4–12. 10.1016/j.exer.2010.09.014 [PubMed: 20883693]

Piljic A, & Schultz C (2006). Annexin A4 self-association modulates general membrane protein mobility in living cells. Molecular Biology of the Cell, 17(7), 3318–3328. 10.1091/mbc.e06-01-0041 [PubMed: 16687573]

Quill B, Irnaten M, Docherty NG, McElnea EM, Wallace DM, Clark AF, & O'Brien CJ (2015). Calcium channel blockade reduces mechanical strain-induced extracellular matrix gene response in lamina cribrosa cells. British Journal of Ophthalmology, 99(7), 1009–1014. 10.1136/bjophthalmol-2014-306093 [PubMed: 25795916]

Rescher U, & Gerke V (2004). Annexins—Unique membrane binding proteins with diverse functions. Journal of Cell Science, 117(Pt 13), 2631–2639. 10.1242/jcs.01245 [PubMed: 15169834]

Reynolds NP, Soragni A, Rabe M, Verdes D, Liverani E, Handschin S, Riek R, & Seeger S (2011). Mechanism of membrane interaction and disruption by alpha-synuclein. Journal of the American Chemical Society, 133(48), 19366–19375. 10.1021/ja2029848 [PubMed: 21978222]

Ries M, Watts H, Mota BC, Lopez MY, Donat CK, Baxan N, Pickering JA, Chau TW, Semmler A, Gurung B, Aleksynas R, Abelleira-Hervas L, Iqbal SJ, Romero-Molina C, Hernandez-Mir G, d'Amati A, Reutelingsperger C, Goldfinger MH, Gentleman SM, … Sastre M (2021). Annexin

A1 restores cerebrovascular integrity concomitant with reduced amyloid-beta and tau pathology. Brain, 144(5), 1526–1541. 10.1093/brain/awab050 [PubMed: 34148071]

Rogers R, Dharsee M, Ackloo S, & Flanagan JG (2012). Proteomics analyses of activated human optic nerve head lamina cribrosa cells following biomechanical strain. Investigative Ophthalmology & Visual Science, 53(7), 3806–3816. 10.1167/iovs.11-8480 [PubMed: 22589438]

Rogers RS, Dharsee M, Ackloo S, Sivak JM, & Flanagan JG (2012). Proteomics analyses of human optic nerve head astrocytes following biomechanical strain. Molecular & Cellular Proteomics, 11(2), M111012302. 10.1074/mcp.M111.012302

Ruan L, Huang HS, Jin WX, Chen HM, Li XJ, & Gong QJ (2013). Tetrandrine attenuated cerebral ischemia/reperfusion injury and induced differential proteomic changes in a MCAO mice model using 2-D DIGE. Neurochemical Research, 38(9), 1871–1879. 10.1007/s11064-013-1093-1 [PubMed: 23780673]

Shrivastava AN, Aperia A, Melki R, & Triller A (2017). Physico-pathologic mechanisms involved in neurodegeneration: Misfolded protein-plasma membrane interactions. Neuron, 95(1), 33–50. 10.1016/j.neuron.2017.05.026 [PubMed: 28683268]

Sigal IA, Flanagan JG, Tertinegg I, & Ethier CR (2004). Finite element modeling of optic nerve head biomechanics. Investigative Ophthalmology & Visual Science, 45(12), 4378–4387. 10.1167/iovs.04-0133 [PubMed: 15557446]

Sigal IA, Flanagan JG, Tertinegg I, & Ethier CR (2007). Predicted extension, compression and shearing of optic nerve head tissues. Experimental Eye Research, 85(3), 312–322. 10.1016/j.exer.2007.05.005 [PubMed: 17624325]

Sigal IA, Grimm JL, Jan NJ, Reid K, Minckler DS, & Brown DJ (2014). Eye-specific IOP-induced displacements and deformations of human lamina cribrosa. Investigative Ophthalmology & Visual Science, 55(1), 1–15. 10.1167/iovs.13-12724 [PubMed: 24334450]

Skrahina T, Piljic A, & Schultz C (2008). Heterogeneity and timing of translocation and membrane-mediated assembly of different annexins. Experimental Cell Research, 314(5), 1039–1047. 10.1016/j.yexcr.2007.11.015 [PubMed: 18164291]

Stowell C, Burgoyne CF, Tamm ER, & Ethier CR, Lasker/IRRF Initiative on Astrocytes and Glaucomatous Neurodegeneration Participants. (2017). Biomechanical aspects of axonal damage in glaucoma: A brief review. Experimental Eye Research, 157, 13–19. 10.1016/j.exer.2017.02.005 [PubMed: 28223180]

Tehrani S, Johnson EC, Cepurna WO, & Morrison JC (2014). Astrocyte processes label for filamentous actin and reorient early within the optic nerve head in a rat glaucoma model. Investigative Ophthalmology & Visual Science, 55(10), 6945–6952. 10.1167/iovs.14-14969 [PubMed: 25257054]

Togo T, Krasieva TB, & Steinhardt RA (2000). A decrease in membrane tension precedes successful cell-membrane repair. Molecular Biology of the Cell, 11(12), 4339–4346. 10.1091/mbc.11.12.4339 [PubMed: 11102527]

Voorhees AP, Jan NJ, Austin ME, Flanagan JG, Sivak JM, Bilonick RA, & Sigal IA (2017). Lamina cribrosa pore shape and size as predictors of neural tissue mechanical insult. Investigative Ophthalmology & Visual Science, 58(12), 5336–5346. 10.1167/iovs.17-22015 [PubMed: 29049736]

Waddell LB, Lemckert FA, Zheng XF, Tran J, Evesson FJ, Hawkes JM, Lek A, Street NE, Lin P, Clarke NF, Landstrom AP, Ackerman MJ, Weisleder N, Ma J, North KN, & Cooper ST (2011). Dysferlin, annexin A1, and mitsugumin 53 are upregulated in muscular dystrophy and localize to longitudinal tubules of the T-system with stretch. Journal of Neuropathology & Experimental Neurology, 70(4), 302–313. 10.1097/NEN.0b013e31821350b0 [PubMed: 21412170]

Wakatsuki T, Schwab B, Thompson NC, & Elson EL (2001). Effects of cytochalasin D and latrunculin B on mechanical properties of cells. Journal of Cell Science, 114(Pt 5), 1025–1036. [PubMed: 11181185]

Weinreb RN, Leung CK, Crowston JG, Medeiros FA, Friedman DS, Wiggs JL, & Martin KR (2016). Primary open-angle glaucoma. Nature Reviews Disease Primers, 2, 16067. 10.1038/nrdp.2016.67

Yamashita T, Nagano K, Kanasaki S, Maeda Y, Furuya T, Inoue M, Nabeshi H, Yoshikawa T, Yoshioka Y, Itoh N, Abe Y, Kamada H, Tsutsumi Y, & Tsunoda S (2012). Annexin A4 is a

possible biomarker for cisplatin susceptibility of malignant mesothelioma cells. Biochemical and Biophysical Research Communications, 421(1), 140–144. 10.1016/j.bbrc.2012.03.144 [PubMed: 22497892]

Yap TE, Davis BM, Guo L, Normando EM, & Cordeiro MF (2018). Annexins in glaucoma. International Journal of Molecular Sciences, 19(4), 1218. 10.3390/ijms19041218 [PubMed: 29673196]

Zhang N, Wang J, Li Y, & Jiang B (2021). Prevalence of primary open angle glaucoma in the last 20 years: A meta-analysis and systematic review. Scientific Reports, 11(1), 13762. 10.1038/s41598-021-92971-w [PubMed: 34215769]

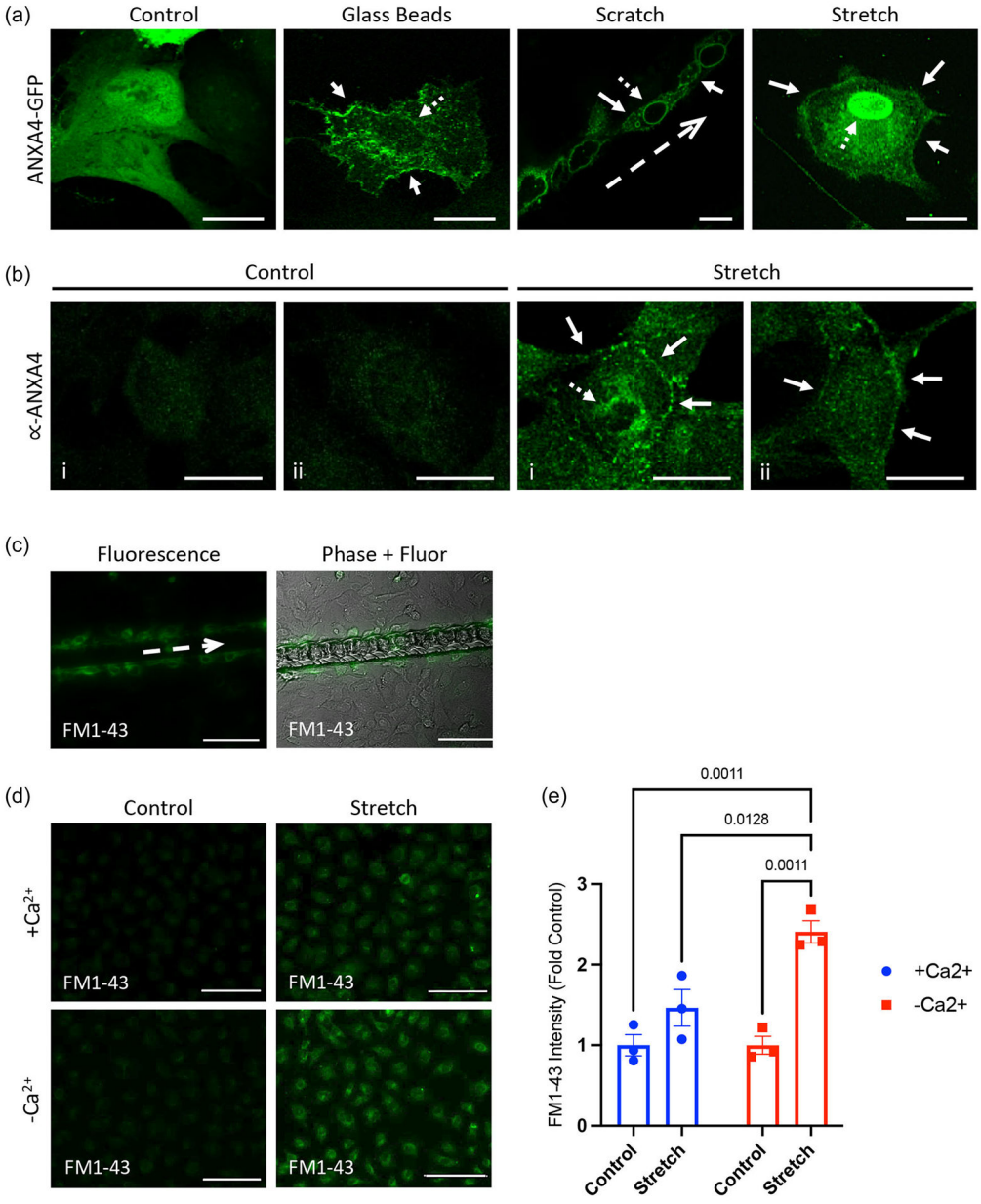

FIGURE 1.

Pathologically relevant biomechanical insult induces rapid ANXA4 translocation and increased cell membrane permeability. (a) GFP tagged ANXA4 was transfected into astrocytic A7 cells and imaged immediately following mechanical injury by glass beads, pipette scratch (dashed line), or after 5 min of 12% stretch. Under control conditions the ANXA4-GFP signal is pancellular and diffuse, but after injury rapidly translocates to cell (arrows) and nuclear (dashed arrows) membrane structures ($n = 3$, scale bars indicate 20 μm). (b) Replicate representative high magnification immunostaining images for endogenous ANXA4 protein under control and stretch conditions after five min reveals increased signal and a similar membrane-localized pattern in stretched cells (arrows, scale bars indicate 20 μm). (c) To test a membrane integrity assay cells were scratched with a

pipette (dashed line), and immediately fixed in the presence of FM 1–43FX dye to visualize the damaged cells (green), in comparison to unaffected neighboring cells observed by phase contrast (Phase + Fluor). (d) To test the impact of biomechanical strain cells were stretched for 5 min at 12% in the presence of FM 1–43FX, with or without Ca^{2+} (scale bars indicate 50 μm). Stretch produced an apparent increase in FM 1–43FX signal in both Ca^{2+} conditions compared to nonstretched controls (green, scale bars indicate 50 μm). (D) Corresponding fluorescence intensity was quantified, showing that stretch significantly increased membrane permeability to FM 1–43FX with Ca^{2+}, and that this increase is significantly greater in the absence of Ca^{2+} ($n = 3$, significant p values from two-way ANOVA indicated on chart, bars represent S.E.). ANOVA, analysis of variance.

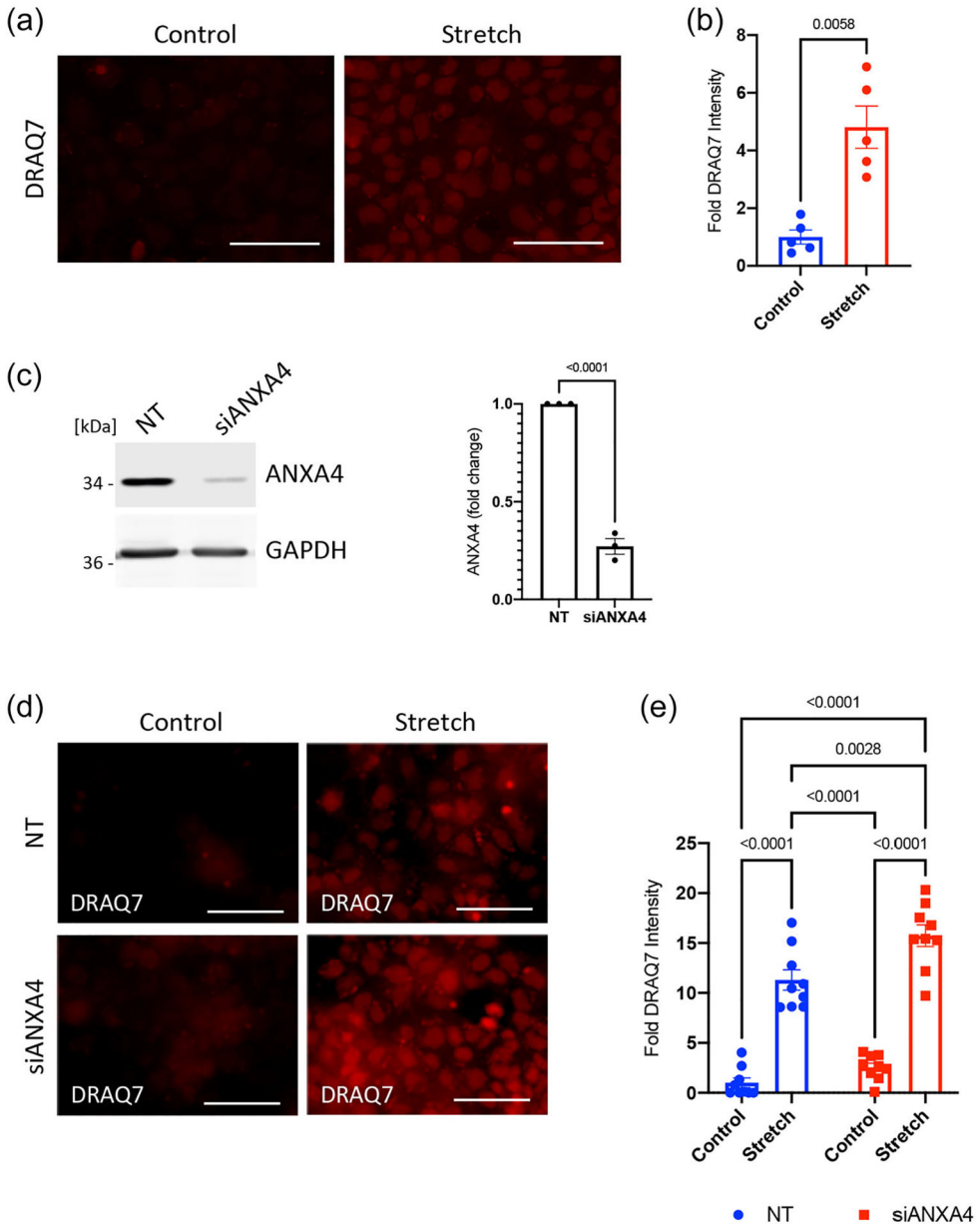

FIGURE 2.

ANXA4 is required for efficient membrane repair during biomechanical stretch. (a) Application of the membrane-impermeable dye DRAQ7 results in increased nuclear signal in A7 cells after 12% stretch (scale bars indicate 50 μm). (b) Corresponding quantification of fluorescence intensity indicates a significant increase in membrane permeability to DRAQ7 following stretch ($n = 5$, p value indicated on chart, bars represent S.E.). (c) Endogenous ANXA4 protein was significantly reduced 75% by siRNA knockdown (siANXA4) compared to nontargeting control (NT) ($n = 3$, p value indicated on chart, bars represent S.E.) (d) Increased DRAQ7 signal was apparent after ANXA4 knockdown under both control and stretch conditions compared to NT controls (scale bars indicate 50 μm). (e) Corresponding quantification of fluorescence intensity showing significantly

increased DRAQ7 membrane permeability following siANXA4 knockdown compared to NT under stretch conditions but not control ($n = 9$, significant p values from two-way ANOVA indicated on chart, bars represent S.E.). ANOVA, analysis of variance; GAPDH, glyceraldehyde 3-phosphate dehydrogenase.

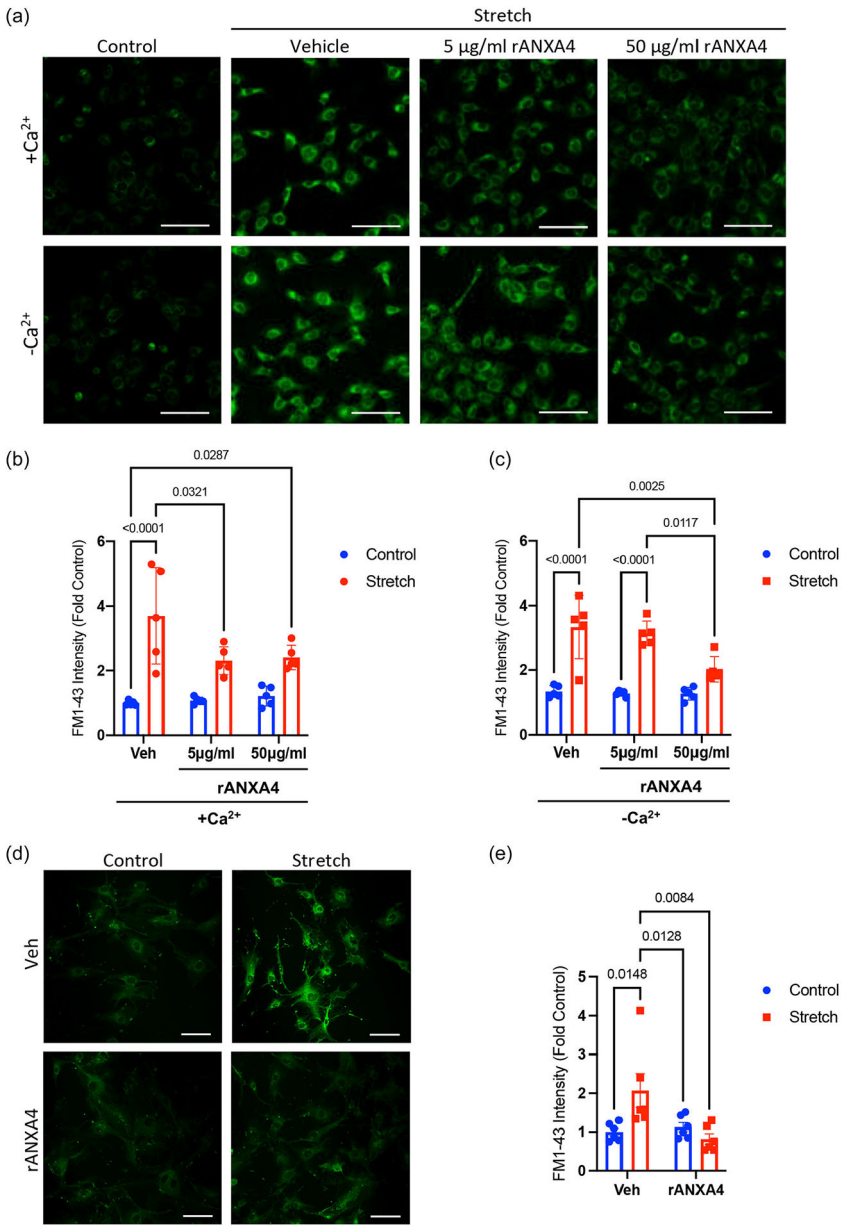

FIGURE 3.

Soluble ANXA4 reduces membrane permeability in a Ca^{2+}-dependent manner. (a) PBS vehicle or recombinant ANXA4 (rANXA4) at 5 and 50 µg/ml were added to cells subjected to 5 min of 12% stretch and imaged with FM 1–43FX (green), under conditions with and without Ca^{2+}. Staining intensity was greater following stretch, indicating increased membrane permeability. However, this increase was abrogated by treatment with increasing concentrations of rANXA4 (scale bars indicate 50 µm). (b) Corresponding quantification of fluorescence intensity for conditions including Ca^{2+} shows significantly reduced FM 1–43FX signal with treatment of both 5 and 50 µg/ml concentrations of rANXA4 compared to vehicle ($n = 5$, significant p values from two-way ANOVA indicated on chart, bars represent S.E.). (c) Quantified fluorescence intensity for conditions without Ca^{2+} only shows

significantly reduced signal at 50 μg/ml rANXA4 ($n = 5$, significant p values from two-way ANOVA indicated on chart, bars represent S.E.). (d) Control or stretched human ONH astrocytes were similarly treated with vehicle or 50 μg/ml rANXA4 and imaged with FM 1–43FX (green), in Ca^{2+}-free media. (e) Corresponding quantification shows significantly increased fluorescence intensity following stretch, and reduced signal with treatment of 50 μg/ml rANXA4 compared to vehicle ($n = 6$, significant p values from two-way ANOVA indicated, bars represent S.E.). ANOVA, analysis of variance; PBS, phosphate-buffered saline.

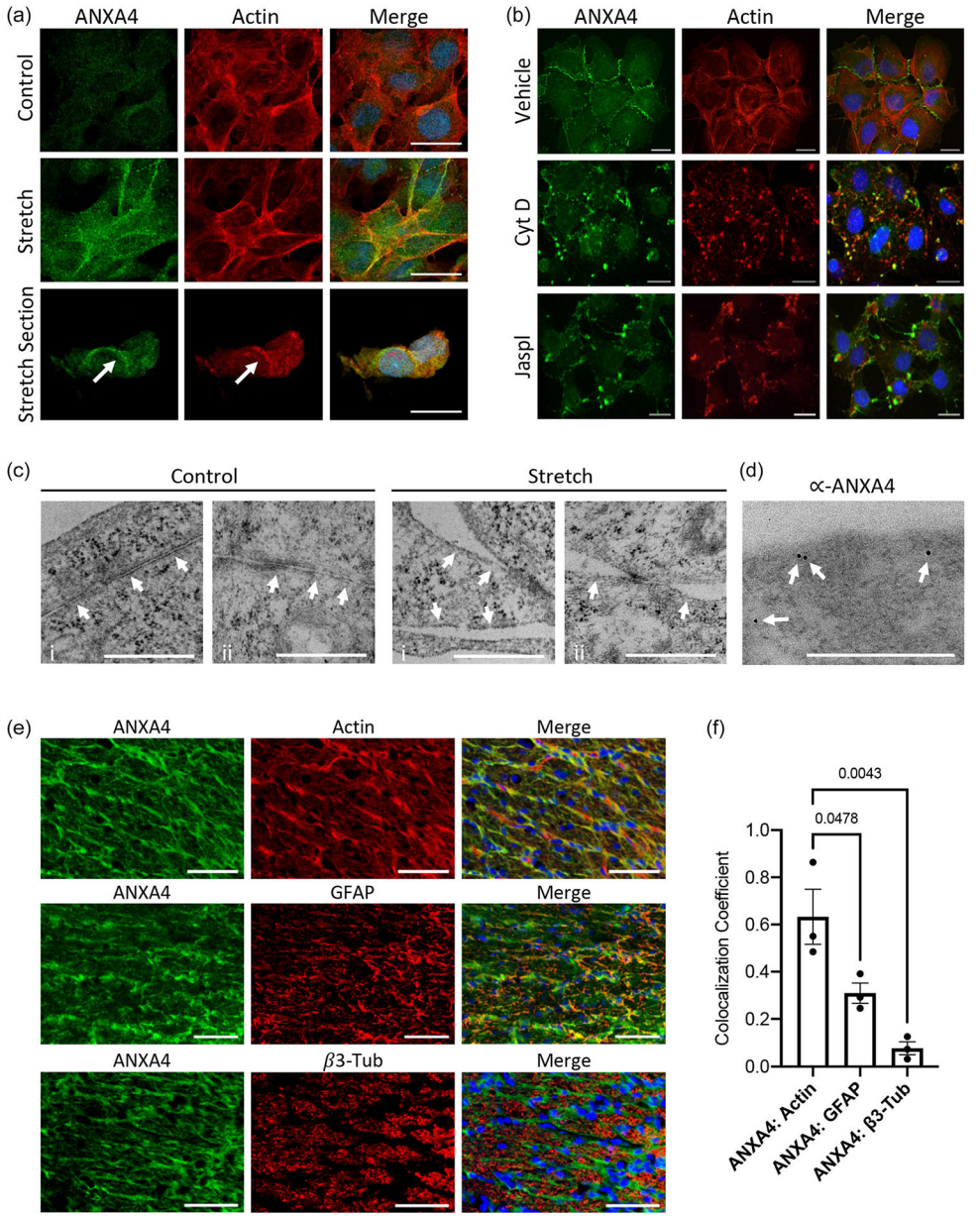

FIGURE 4.

ANXA4 interacts with cortical actin at cell junctions and in the ONH. (a) Control and stretched A7 cells were fixed after 5 min and costained with an antibody against endogenous ANXA4 (green), and for F-actin with rhodamine-phalloidin (red). Stretched cells showed increased ANXA4 signal at cell membranes that partially colocalized with cortical actin, and was prominent along cell junctions. Sections through these stretched cells confirms this localization (arrows) (scale bars indicate 50 μm). (b) Stretched cells were treated with either vehicle, or the actin disruptors 1.0 μM cytochalasin D (Cyt D), or 0.5 μM jasplakinolide (Jaspl) and costained for ANXA4 (green) and F-actin (red). Treatment with either Cyt D or Jaspl disrupted actin staining, and similarly affected ANXA4 localization (scale bars indicate 20 μm). (c) Replicate representative TEM images of control and stretched cell

sections illustrating the appearance of disrupted membranes and tight junctions under stretch conditions (arrows, scale bars indicate 500 nm). (d) Immunogold labeling with ANXA4 antibodies highlighted ANXA4 targeted particles near cell membranes in stretched samples (arrows, scale bar indicates 500 nm). (e) Representative cross sections through a rat ONH at high magnification reveal a colocalization of ANXA4 and F-actin in vivo, partially overlapping with GFAP, and ensheathing β3 tubulin positive nerve fiber bundles (blue staining represents DAPI, scale bars indicate 50 μm). (f) Corresponding colocalization coefficients for each costaining condition confirm this pattern ($n = 3$, significant ANOVA p values indicated on chart, bars represent S.E.). ANOVA, analysis of variance; DAPI, 4′, 6-diamidino-2-phenylindole; GFAP, glial fibrillary acidic protein; ONH, optic nerve head; TEM, transmission electron microscopy.

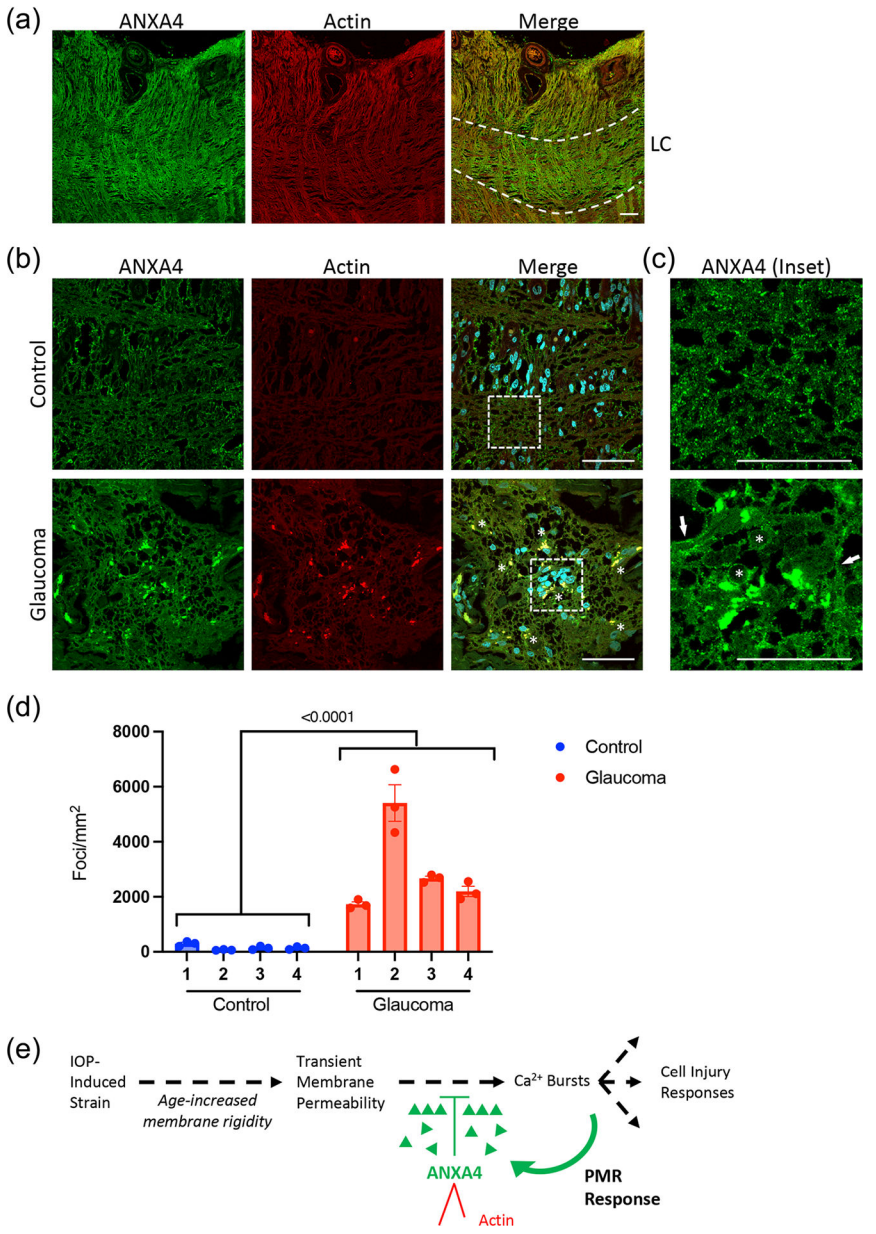

FIGURE 5.

ANXA4 associates with F-actin in the human ONH and relocalizes in glaucomatous tissues. (a) ANXA4 staining (green) is prominent in the human ONH, particularly in the LCr region (dotted lines), and colocalizes with actin (red) (bar indicates 50 μm) (b) Representative ×60 oil immersion images of the LCr region from matched control and glaucoma samples showing the appearance of ANXA4:actin foci in glaucomatous samples (yellow; asterisks, bars indicate 50 μm). (c) Higher resolution images corresponding to the dotted box insets in (b) showing ANXA4 staining patterns in control cells, and increased cell membrane (arrows) and nuclear membrane (asterisks) localization in glaucomatous tissue (bars indicate 50 μm). (d) Quantification of ANXA4:actin foci per mm^2 in three LCr regions for each eye from control and glaucoma patient samples (*p* value between groups indicated on graph, bars

represent S.E.) (e) A proposed cartoon model of Ca^{2+}-induced ANXA4 accumulation at membrane strain injury sites as a component of a glaucomatous PMR response. LCr, lamina cribrosa; ONH, optic nerve head; PMR, plasma membrane repair.